



Single-cell damage elicits regional, nematode-restricting ethylene responses in roots

Peter Marhavý^{1,*} , Andrzej Kurenda¹, Shahid Siddique^{2,†}, Valerie Déneraud Tendon¹, Feng Zhou¹, Julia Holbein², M Shamim Hasan², Florian MW Grundler², Edward E Farmer¹ & Niko Geldner^{1,**} 

Abstract

Plants are exposed to cellular damage by mechanical stresses, herbivore feeding, or invading microbes. Primary wound responses are communicated to neighboring and distal tissues by mobile signals. In leaves, crushing of large cell populations activates a long-distance signal, causing jasmonate production in distal organs. This is mediated by a cation channel-mediated depolarization wave and is associated with cytosolic Ca²⁺ transient currents. Here, we report that much more restricted, single-cell wounding in roots by laser ablation elicits non-systemic, regional surface potential changes, calcium waves, and reactive oxygen species (ROS) production. Surprisingly, laser ablation does not induce a robust jasmonate response, but regionally activates ethylene production and ethylene-response markers. This ethylene activation depends on calcium channel activities distinct from those in leaves, as well as a specific set of NADPH oxidases. Intriguingly, nematode attack elicits very similar responses, including membrane depolarization and regional upregulation of ethylene markers. Moreover, ethylene signaling antagonizes nematode feeding, delaying initial syncytial-phase establishment. Regional signals caused by single-cell wounding thus appear to constitute a relevant root immune response against small invaders.

Keywords ethylene; nematodes; regional response; single-cell laser ablation; surface depolarization

Subject Categories Plant Biology; Signal Transduction

DOI 10.15252/embj.2018100972 | Received 21 October 2018 | Revised 1 March 2019 | Accepted 7 March 2019 | Published online 6 May 2019

The EMBO Journal (2019) 38: e100972

Introduction

Dissecting the molecular events occurring during actual attack of an invading organism is highly challenging because of the complex interplay of pattern-recognition events and damage perception, as well as the manipulation of the host's cellular physiology and immune response by the invader. Understanding plant responses to physical damage in isolation is therefore of crucial importance.

Molecules reporting damage to plant cells, such as cell wall fragments and release of strictly intracellular agents from cells (e.g., ATP, or cytosolic peptides), are thought to be indicators of damage to the plant's cellular integrity (Choi *et al*, 2014; Duran-Flores & Heil, 2016). Yet, such isolated agents are often not sufficient to reproduce the responses occurring upon actual physical damage, although recent data suggest that extracellular glutamate might be a central agent reporting cellular damage (Toyota *et al*, 2018).

Current ways to induce physical damage generally involve destruction of large populations of cells, affecting most or all of the cell types in a given organ (Mousavi *et al*, 2013; Toyota *et al*, 2018). While this has been powerful to elicit and study the systemic alarm signals to other organs, it has the shortcoming of confounding responses from many different cell types. In addition, it is only an appropriate simulation of damage caused by big insects or vertebrate herbivores, but might not be a good reflection of the more restricted and precise damage caused by a plethora of other attackers, such as small insects, nematodes, or necrotrophic microbes. We therefore pioneered single-cell laser ablations as a potentially powerful addition to the currently used techniques in order to understand the fundamental mechanisms of damage perception in plants.

Arabidopsis seedling roots allow live observations and manipulations at exquisite resolution and precision. While they are popular for investigations in cell biology, development, and hormone perception (Benfey & Scheres, 2000), their use in investigating basic aspects of plant–pathogen interactions and plant defense responses has been more limited. This not only leads to a severe lack of understanding of the specificities of root versus leaf defense responses, but also represents a lost opportunity to harness the specific advantages of roots as models for understanding plant defense responses.

In recent years, breakthroughs in root microbiome research have led to an increased interest in understanding root defense responses in the larger context of root biotic interactions (Hacquard *et al*, 2017). In a recent collaborative effort, we have generated a set of defense response marker lines, consisting of promoters responsive to major stress and defense response pathways driving a NLS triple mVenus fusion that allows for highly sensitive and cell type-specific readouts (Poncini *et al*, 2017). Combining these with our ability for single-cell laser ablation in roots (Marhavý *et al*, 2016), pioneered

¹ Department of Plant Molecular Biology, Biophore, UNIL-Sorge, University of Lausanne, Lausanne, Switzerland

² Department of Molecular Phytomedizin, Rheinische Friedrich-Wilhelms-University of Bonn, Bonn, Germany

*Corresponding author. Tel: +41 21 692 4191; E-mail: peter.marhavy@unil.ch

**Corresponding author. Tel: +41 21 692 4192; E-mail: niko.geldner@unil.ch

[†] Present address: Department of Nematology and Entomology, University of California, Davis, Davis, CA, USA

by van den Berg *et al* (1997), we set out to explore the specific responses of roots to precise cellular damage.

Results

Single-cell damage induces regional ethylene, but not jasmonate or salicylic acid production and response

In leaves, mechanical crushing of large cell populations leads to membrane depolarization and jasmonate production in damaged as well as undamaged tissues (Mousavi *et al*, 2013). We investigated whether precise wounding of single cells using an infrared (IR) laser in the root would cause similar physiological responses. At first, we analyzed the jasmonic acid marker lines *pJAZ10::NLS-3xVenus* and *pAOS::NLS-3xVenus* (Park *et al*, 2002; Poncini *et al*, 2017), the JAS9-YFP jasmonate biosensor (Larrieu *et al*, 2015), and the salicylic acid marker line *pPRI::NLS-3xVenus* (Poncini *et al*, 2017). After ablation of cortex cells in 5-day-old roots, neither jasmonate nor salicylic acid reporter lines showed any consistent responses within 10 h (Fig 1A–L; Appendix Fig S1A–D). We confirmed functionality of jasmonate and salicylic acid marker lines by treating roots with 1 μ M methyl jasmonate (MeJA) and 1 μ M salicylic acid (SA). All jasmonate marker lines respond to MeJA treatment in roots (Fig 1A–L). Interestingly, the *pPRI::NLS-3xVenus* did not show any increase of signal in roots after treatment with 1 μ M SA (Appendix Fig S1A–D). Yet, strong induction of *pPRI::NLS-3xVenus* expression could be observed in the cotyledons, confirming functionality of the line and suggesting that SA elicits a root response different from that in leaves (Appendix Fig S1E and F). In order to investigate whether the lack of jasmonate response observed is due to the fact that only single cells are damaged in our experiments, we mechanically crushed large population of root cells, similar to standard wounding done on leaves. Crushing of root tips (Appendix Fig S1G) induced jasmonate production and response genes to some degree, as visualized by our *JAZ10*, *AOS* reporter, and an additional *LOX6::GUS* reporter. LIPOXYGENASE 6 has been shown to be the major LOX enzyme for jasmonate production in roots (Grebner *et al*, 2013; Gasperini *et al*, 2015a, b). However, none of the markers showed a consistent, robust induction; i.e., only a fraction of the roots responded and with an amplitude much lower (Appendix Fig S1H–L) than seen upon jasmonate treatment (Fig 1A–H). The non-transcriptional, normalized intensity JAS9 jasmonate sensor did not show any measurable

response upon ablation (Fig 1I). Contrasting this, ablation of single epidermal cells of cotyledons did lead to a consistent induction of the *pJAZ10::NLS-3xVenus* (Fig 1M and N, Movie EV7). Thus, the paradigmatic jasmonate induction upon wounding observed in aerial tissues does not appear to play a similarly predominant role in roots. We then analyzed two markers reporting ethylene synthesis and signaling, *pACS6::NLS-3xVenus* and *pPR4::NLS-3xVenus* (Liu & Zhang, 2004; Proietti *et al*, 2011), both of which we confirmed to be expressed and functional in roots (Appendix Fig S2A–F). Here, both lines responded to cortex cell ablations in the root (Fig 2A–D; Appendix Figs S2A–F and S3C–J). Consistent with previously reported expression and response patterns (Tsuchisaka & Theologis, 2004), *ACS6* responses were not exclusive to, but very much biased toward, stele tissues, while *PR4* responses were largely confined to the endodermis. *ACS6* was also robustly induced by crushing of root tips, contrasting with the inconsistent induction of jasmonate markers described above (Appendix Fig S2G–I). Time-lapse imaging revealed that 2–3 h after cortex ablation, both *pACS6::NLS-3xVenus* signal intensity and the number of cells with mVenus signal increased significantly compared to control (Appendix Fig S3). However, time-lapse imaging itself causes significant induction of the ethylene-response genes in controls, partially leveling out the ablation response (Appendix Fig S3C–J). For unknown reasons, propidium iodide (PI) cell wall staining during imaging alleviated this problem (compare Appendix Fig S3C and D). We nevertheless avoided both long-term time-lapse imaging and use of PI in most experiments and confined ourselves to one time point, thus keeping background induction to a minimum. Interestingly, when measuring the spatial extent of the response, we found that our single-cell ablations upregulated *ACS6* and *PR4* in a regional, but non-systemic, fashion, encompassing a region of about 500 μ m for *ACS6* (Appendix Fig S4A and B). Cell ablation of a single cortical cell thus appears to be able to induce stress hormone production and response in a considerable number of neighboring endodermis and stele cells and to extend bi-directionally along the root axis over a number of cellular distances, begging the question as to the nature of the mobile signal that could mediate this effect.

Single-cell ablation causes a regional surface depolarization of roots

Wound signals eliciting stress responses in unwounded cells have been described for decades, yet the nature of the mobile agent and

Figure 1. Jasmonate does not respond to single-cell laser ablation.

A–H Propidium iodide (PI) staining of roots (red) allowed visualization of cell death (white arrowhead) by increase in PI fluorescence. (A–C, E–G) Real-time monitoring of 4D (xyzt) maximum projection images of jasmonate response marker lines *JAZ10::NLS-3xVenus* (A–C) and *AOS::NLS-3xVenus* (E–G) in the *Arabidopsis* root after laser ablation of cortex cells (C, G) on 1 μ M methyl jasmonate (MeJA) treatment (B, F). Time-lapse images of representative movies are shown. (A, C) *JAZ10::NLS-3xVenus* showed no response, either in control roots or after ablation ($n = 20$ roots each). (E, G) *AOS::NLS-3xVenus* showed weak signals in 5 roots ($n = 20$) after ablation (G), similar to numbers in non-ablated controls, where 5 roots ($n = 17$) showed signals. (B, F) Both jasmonate markers showed responses in roots upon 1 μ M MeJA treatment ($n = 20$). (D, H) Graphical representation of quantification of movies shown in (A–C, E–G), respectively.

I–L Ratiometric *35S::JAS9-Venus H2B-RFP* biosensor in the *Arabidopsis* root before/after laser ablation of cortex cells (I) or treated with 1 μ M MeJA (L). No response was observed after 20 min, either in control roots or after ablation, while the sensor responded to treatment with 1 μ M MeJA, but not to a water control (J). (K, L) Representative picture of experiments quantified in (J). Graphs combine data from 2 experiments with $n = 10$ roots (error bars indicate standard error; $**P < 0.002$, the significance was determined by *t*-test).

M, N XYZ maximum projection images show the expression of *JAZ10::NLS-3xVenus* in PI-stained *Arabidopsis* cotyledons before (M) and after ablation (N). Expression of *JAZ10::NLS-3xVenus* was observed in 8 cotyledons ($n = 9$) in ablated and 1 cotyledon ($n = 7$) in non-ablated control. A white arrow indicates an ablated epidermal cell, and yellow arrows indicate nuclear *JAZ10::NLS-3xVenus* signals. Time points are indicated at the top right corner of each frame.

Data information: Scale bar, (A–C, E–G, K, L) 70 μ m and (M, N) 100 μ m.

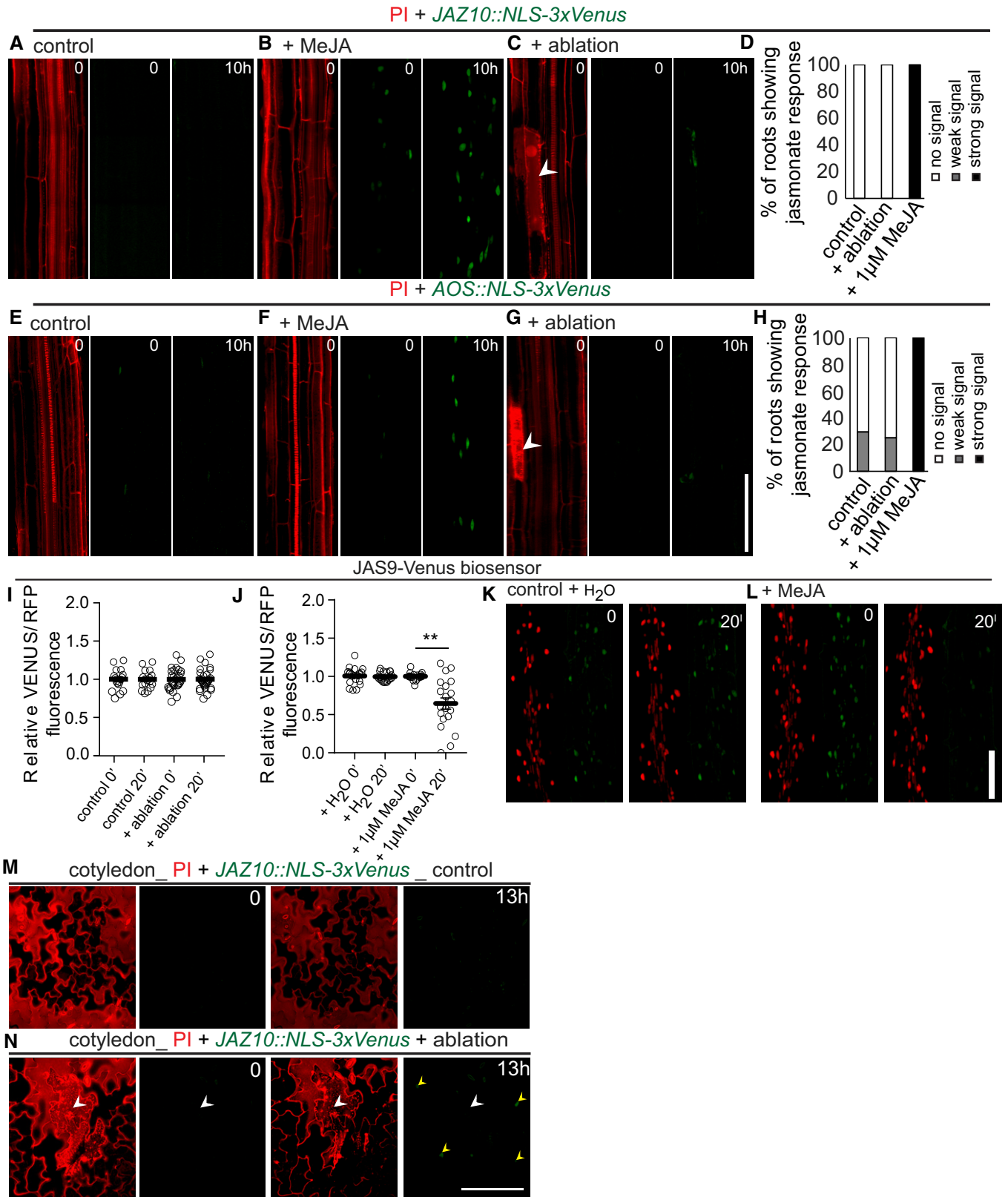


Figure 1.

the mechanism of signal propagation have often remained hotly debated. One common feature that has emerged to be associated with—and required for—transmission of diverse stress signals is a propagating increase of intracellular calcium, ROS production, and membrane depolarization (Gilroy *et al*, 2014). Often, such signals are of systemic nature, i.e., propagating through an entire organ or plant. Yet, their elicitation also involves exposure of a large group of cells to a stress, such as parts of one leaf or an entire root meristem. We wondered whether the exquisitely localized damage of one cell and the more restricted ethylene response we observe would also be associated with the same trio of molecular events. We therefore placed a non-invasive electrode on the root surface (epidermis), opposite to the side of cell ablation (Fig 2E). Upon ablation, we measured surface potential changes of -79.5 ± 6.4 mV (Fig 2F and G). Interestingly, these depolarization spikes triggered by laser ablation of single cells are of comparable amplitude to those measured in aerial tissues (Mousavi *et al*, 2013), although of much shorter duration. We also mapped the distance over which the electrical signal would be transmitted and found that it was still detectable at 200 μm , but absent beyond 400 μm (Fig 2H), strongly differing from the centimeter distances measured in aerial parts of the plants (Mousavi *et al*, 2013). In order to exclude that these surface potential changes were simply a result of the heat load applied by the two-photon laser, we performed “mock ablations” on the growth medium in close proximity to the root (Fig 2I, red arrowhead). Media heating by the laser only caused small changes (Fig 2I, red arrowhead), not comparable to those induced by cell ablation (Fig 2I, black arrowhead). The same was true for applying IR laser at doses that only heated, but did not ablate cortex cells (Fig 2J). The lag between the end of the 2-s laser pulse and the depolarization peak was 1.5 ± 0.6 s, translating into a maximal estimated signal speed of 85 $\mu\text{m}/\text{s}$, assuming a distance of 128 μm between ablated cortex cell and electrode, and a minimal speed of 37 $\mu\text{m}/\text{s}$, assuming immediate ablation of the cortex at the beginning of the pulse (Fig 2K and L).

The short-distance electric signaling depends on multiple ion channel activities

Changes in ion channel and pump activities are the major determinants of cell membrane electrical changes in plants (Pickard &

Ding, 1993; Véry & Sentenac, 2002; Shomer *et al*, 2003; Kinraide, 2006; Mishra *et al*, 2013; Lim *et al*, 2015; Catterall *et al*, 2017; Flucher & Tuluc, 2017; Perez Garcia *et al*, 2017). Indeed, calcium channel inhibitors, such as methoxyverapamil or GdCl_3 , efficiently reduced or blocked depolarization after cell ablation, as did inhibitors of chloride and potassium channels and proton pumps (Fig 3A and B). Fusicoccin, by contrast, a well-described activator of plant plasma membrane proton pumps (Würtele *et al*, 2003), did not reduce, but rather enhanced the depolarization amplitude after ablation (Fig 3C). These results suggest that the known major ions underlying plant cell transmembrane potentials are also required for the ablation-induced depolarization that we observe here. Interestingly, the glutamate receptor-like channels GLR3.3 and GLR3.6, shown to be necessary for transmitting surface potential changes to distal leaves after leaf wounding (Mousavi *et al*, 2013), were not involved in mediating the regional depolarization after single-cell ablation observed here (Appendix Fig S5A), suggesting that other GLR family members might mediate this calcium inhibitor-sensitive depolarization.

Single-cell ablation induces regional calcium waves

Stress stimuli such as PAMPs, salt, or mechanical damage have been shown to induce a Ca^{2+} wave that travels through the root for long distances (Steinhorst & Kudla, 2014; Choi *et al*, 2016; Gilroy *et al*, 2016). A number of genetically encoded live-imaging probes for intracellular calcium are available (Albrecht *et al*, 2003; Pandey *et al*, 2004; Monshausen *et al*, 2008; Matzke & Matzke, 2015), and we chose the widely used, intensometric R-GECO1 (Keinath *et al*, 2015) sensor as well as the intensity-based concentration sensor Case12 (Matzke & Matzke, 2015) in order to test whether we could observe a local Ca^{2+} wave upon single-cell laser ablation. We performed ablation of cortical cells in R-GECO lines (Fig 3D–I and Movie EV1). Interestingly, we could observe Ca^{2+} wave propagation starting at the ablation side, arriving with a slight delay at the opposite cortex side (Fig 3E, Movie EV1). When the cortical signals have already dissipated, a slower, more persistent propagation of the calcium signal was observed within the stele (Movie EV1). Increases of calcium signal could also be

Figure 2. Single-cell ablation induces ethylene responses and local surface depolarization.

- A, B 3D tile-scan (xyz) maximum projection images of *ACS6::NLS-3xVenus* ethylene biosynthesis marker line in the *Arabidopsis* root. Time points at the top right corner of each frame. Non-ablated control root (A) and root with cortex cell ablation (B). White arrowhead indicates position of ablated cell. Representative pictures of experiments quantified in (C, D).
- C, D Laser ablation of single cortex cells induces ethylene biosynthesis marker *ACS6* (*ACS6::NLS-3xVenus*), visualized as increases of number of cells with detectable nuclear signal (C), or increase in average signal intensity (D) (** $P < 0.001$, the significance was determined by *t*-test, pool of three repeats with $n = 5$ roots).
- E Schematic representation of experimental setup for detecting surface potential changes after laser ablation.
- F, G Electrophysiological recording of surface potential changes measured with a non-invasive electrode placed on the root surface with or without laser ablation of cortex cells. Laser ablation-induced depolarization, amplitude in mV (G) quantification of depolarization amplitude (*** $P < 0.0005$, the significance was determined by *t*-test, pool of three repeats with $n = 21$ roots).
- H Surface potential changes over varying distances of different cortex cells within the same root. Arrowheads indicate the distance of electrode placement from the ablation site.
- I–L Average lag time of maximum depolarization after laser ablation ($n = 31$ roots). (K) Representative read of experiments quantified in (J). Duration of laser pulse indicated by black lines; red lines indicate lag between maximum depolarization and the end of laser pulse. (I, L) Comparison of surface potential changes caused by laser ablation of cortex cells (black arrowheads) with effect of application of the same laser power on (I) media next to the root and (L) on the cortex cell with reduced laser power (red arrowhead).

Data information: Error bars in C, D, G, and K indicate 95% confidence interval (CI) around mean. Scale bar: (A, B) 100 μm . See also Fig 4, Appendix Fig S2, and Appendix Fig S3.

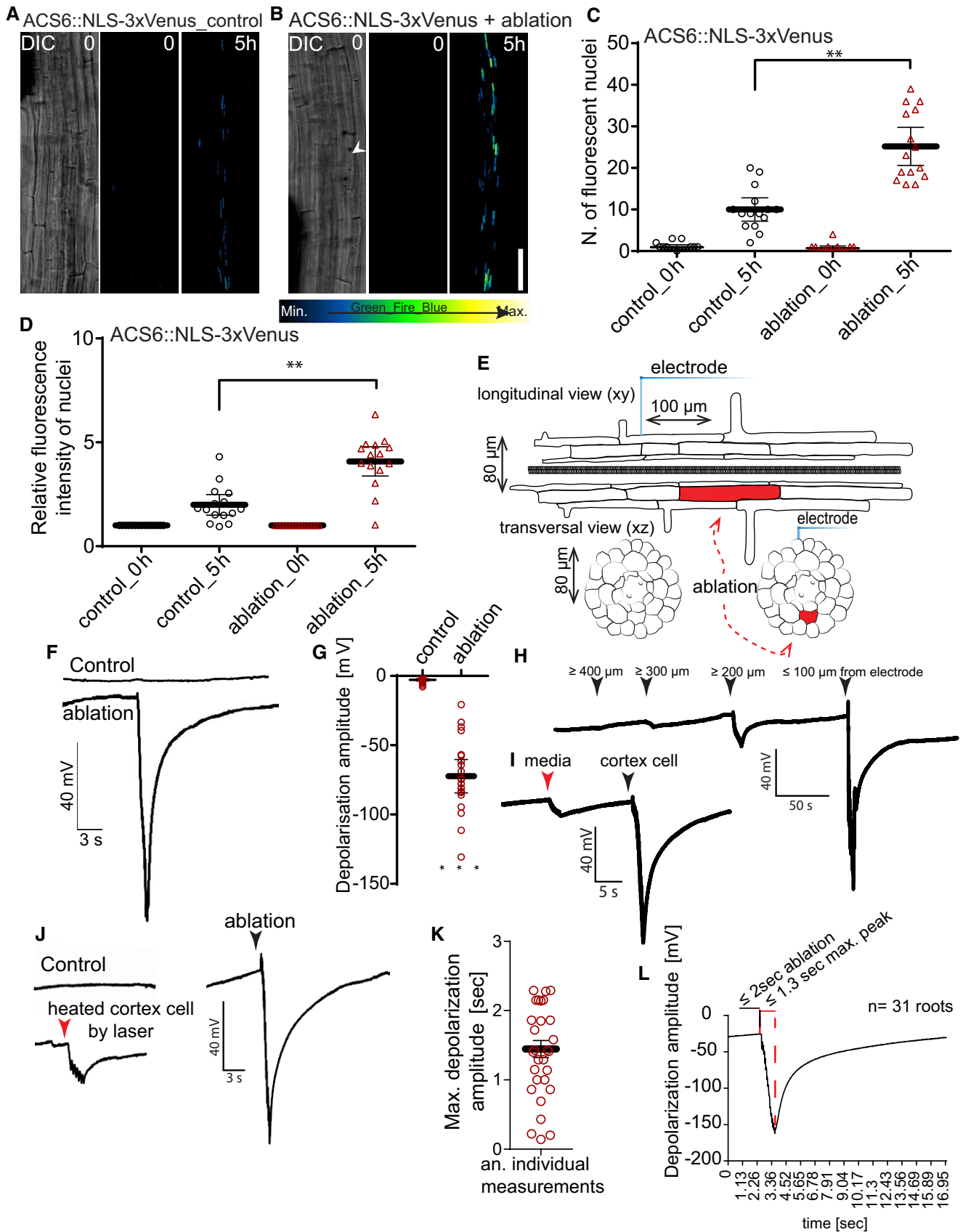


Figure 2.

observed upon crushing of entire root tips (Appendix Fig S6A and B). Upon mere heating of single cells, the Ca^{2+} signal was weaker and stayed confined to the heated cell (Fig 3G, Movie EV6), similar to touch-induced calcium responses (Monshausen *et al*, 2009).

Both basal and ablation-induced R-GECO signals were abrogated upon $GdCl_3$ treatment of roots (Fig 3H–I). Using the Case12 marker (Appendix Fig S5B–E) gave very similar results than those using R-GECO.

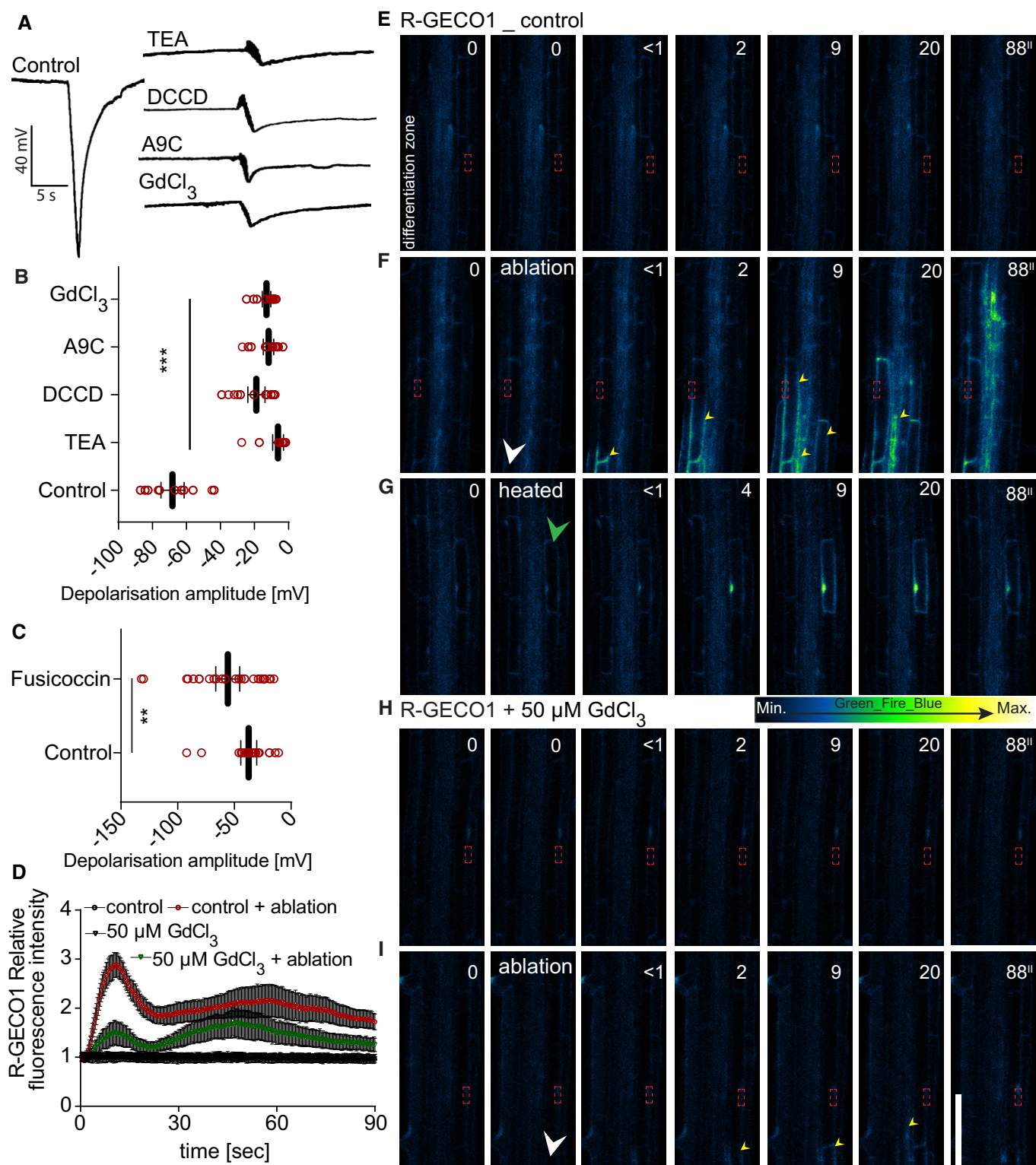


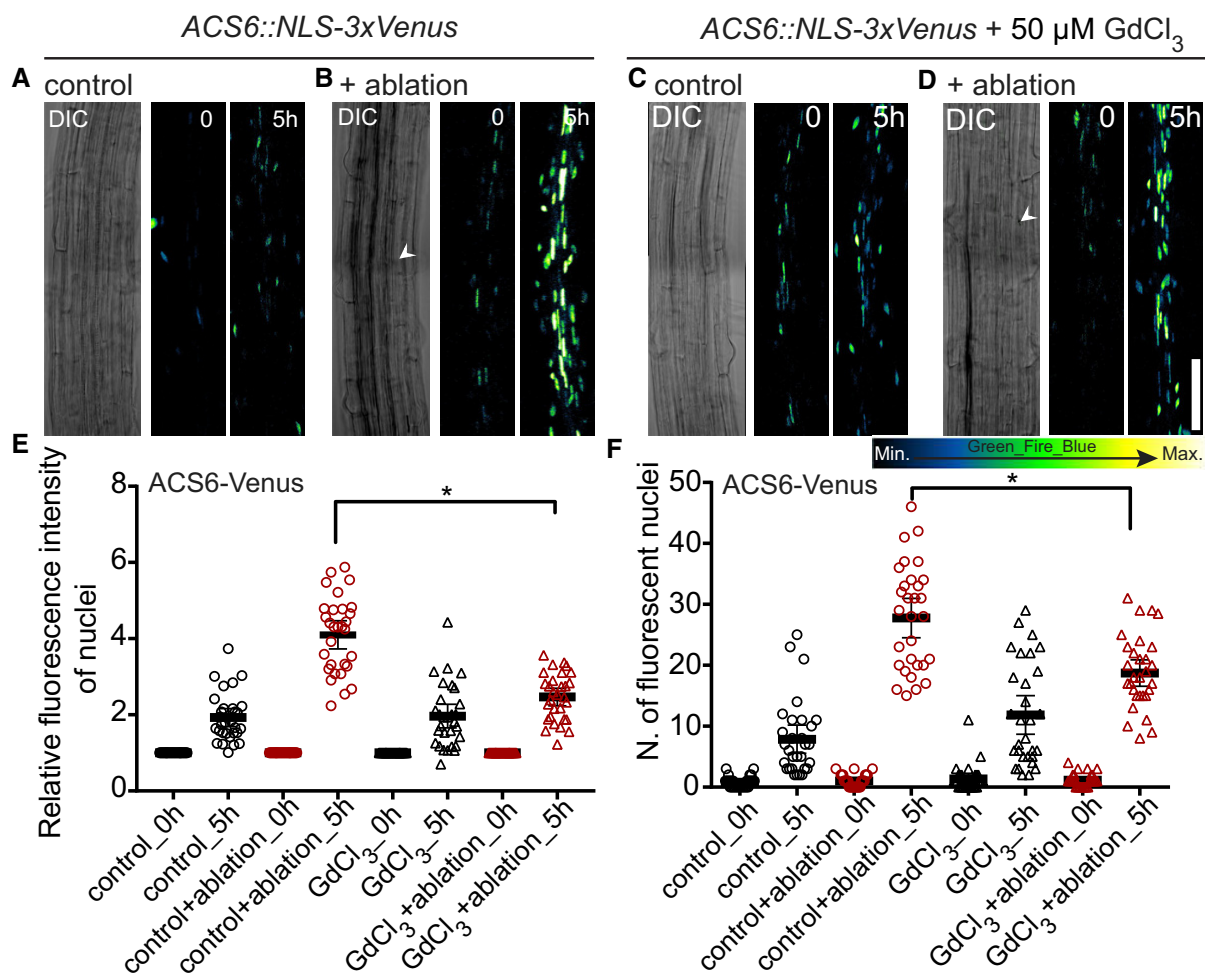
Figure 3.

Figure 3. Ion channel inhibitors affect ablation-induced depolarization and cytosolic calcium increases.

A–C Recording and quantification of surface depolarization amplitudes in 5-day-old *Arabidopsis* roots after cortex cell ablation under ion channel inhibitor and fusicoccin treatments. Anthracene-9-carboxylic acid (A9C, 50 μ M): chloride channel blocker; $GdCl_3$ (50 μ M): calcium channel blocker; vanadate (50 μ M): non-specific pump inhibitor; N,N-dicyclohexylcarbodiimide (DCCD, 50 μ M): proton channel blocker, proton pump inhibitor; tetraethylammonium (TEA, 50 μ M): potassium channel blocker; (C) fusicoccin (5 μ M): proton pump activator; (B, C) quantification of read examples shown in (A) (** $P < 0.005$, *** $P < 0.0005$; the significance was determined by *t*-test, $n = 15$ –20 roots, repeated three times; error bars indicate mean value with 95% CI).

D–I Real-time monitoring and quantification (D) of calcium wave propagation after cortex cell ablation using a *R-GECO1* reporter line (repeated two times, each with $n = 20$ roots); error bars indicate standard error, and time-lapse images of representative movies are shown. (E, F) Comparison of calcium wave caused by laser ablation of cortex cells (F) with effect of reduced laser power (heated) application on the cortex cell (G). (E–I) Time points in seconds (") at the top right corner of each frame. Signal increases after ablation at opposite root side show slight lag compared to ablated root side. In non-ablated control roots, no increases of signal were observed; the same applies for 50 μ M $GdCl_3$ -treated roots after ablation. White arrowheads indicate ablation position, green arrowhead indicates heated cell, yellow arrowheads indicate calcium wave propagation, and red frame indicates region of signal quantification in (D).

Data information: Scale bar: (E–I) 100 μ m. See also Figure 5, Appendix Fig S5, and Movie EV1.

**Figure 4. Laser ablation-induced ethylene responses are partially dependent on calcium increases.**

A–D XYZ maximum projection images of *ACS6::NLS-3xVenus* ethylene biosynthesis marker line in the *Arabidopsis* root after laser ablation with or without $GdCl_3$ (50 μ M). Time points in hours (h) at the top right corner of each frame. White arrowheads indicate position of cortex cell ablation. Representative pictures are shown.

E, F Signal intensity quantification and number of cells with positive nuclear (NLS-3xVenus) signal increases after ablation in control, but increases are reduced upon $GdCl_3$ (50 μ M) inhibitor treatment (* $P < 0.05$, the significance was determined by *t*-test, data pooled from three independent experiments with $n = 10$ roots each; error bars indicate mean value with 95% CI).

Data information: Scale bar, (A–D) 100 μ m.

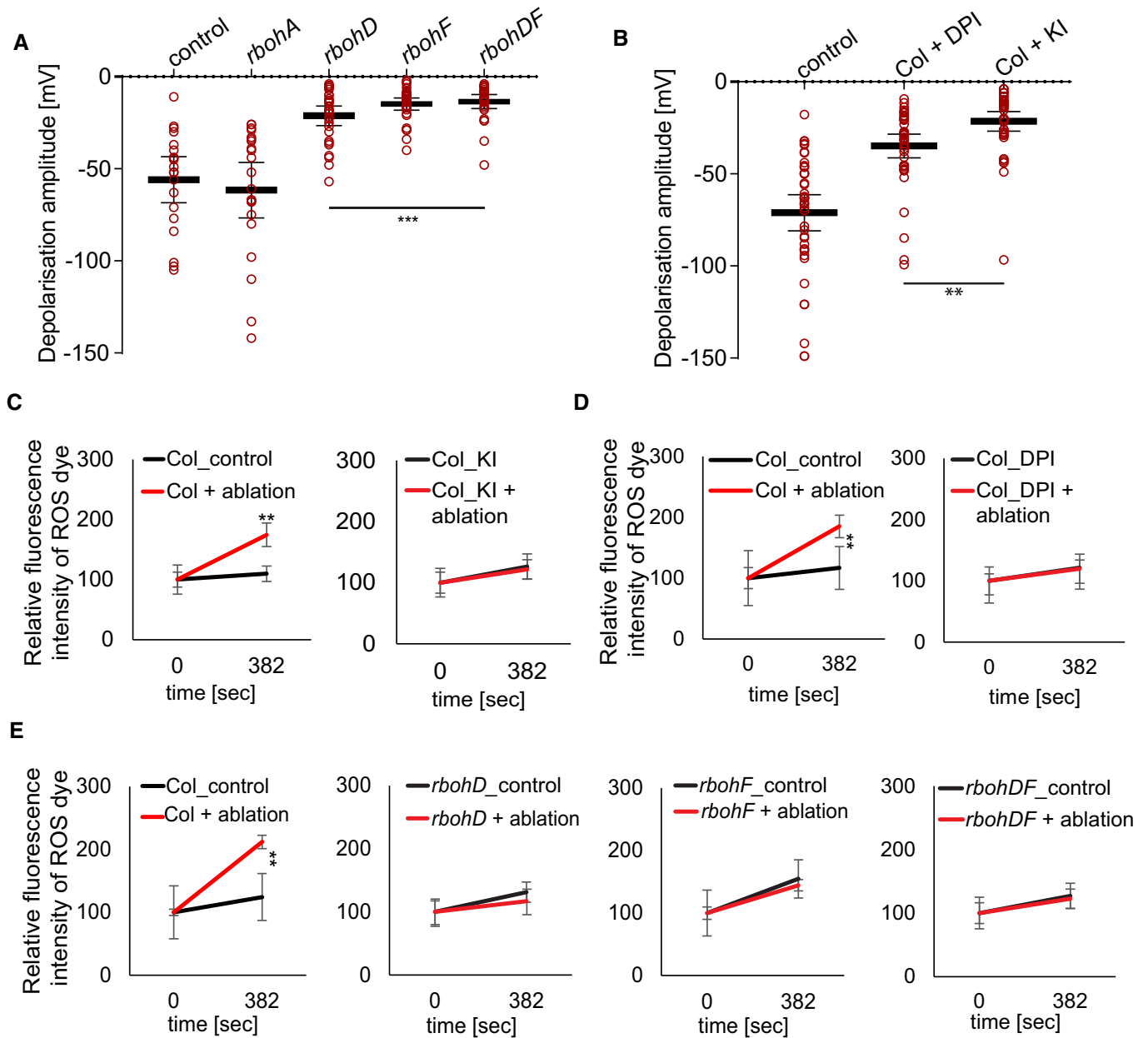


Figure 5. Laser ablation-induced depolarization and ROS increases require NADPH oxidases.

A, B Quantification of surface potential changes after laser ablation of root cortex cells. (A) Quantification of depolarization amplitudes after cortex cell ablation in *rbohD*, *rbohF*, and *rbohDF* mutants, but not in *rbohA*, compared to control ($***P < 0.0005$, the significance was determined by *t*-test, data pooled from three independent experiments with $n = 10$ roots each; error bars indicate mean value with 95% CI). (B) Application of ROS production inhibitor diphenyleneiodonium (DPI, 10 μM) and ROS scavenger potassium iodide (KI, 5 mM) significantly reduced depolarization amplitude, compared to non-treated control ($**P < 0.005$; the significance was determined by *t*-test, data pooled from three independent experiments with $n \geq 10$ roots each; error bars indicate mean value with 95% CI).

C–E Quantification of ROS production after single-cell laser ablation. For ROS visualization, 20 μM 2',7'-dichlorodihydrofluorescein diacetate (H2DCFDA) was used; representative images are shown in Appendix Fig S4F–Q ($**P < 0.005$, data pooled from three independent experiments with $n = 5$ roots each; error bars indicate standard error).

Calcium and ROS both contribute to local, damage-induced ethylene responses

We next tested whether inhibiting cytosolic calcium increases would suppress induction of ethylene-response markers upon cell ablation.

Indeed, after ablation of cortex cells, *pACS6::NLS-3xVenus* response was attenuated in GdCl_3 -treated seedlings (Fig 4A–F), indicating that cytosolic calcium increases contribute to, but are not fully required for induction of ethylene responses in neighboring cells. Similar to calcium, increases in reactive oxygen species (ROS) can

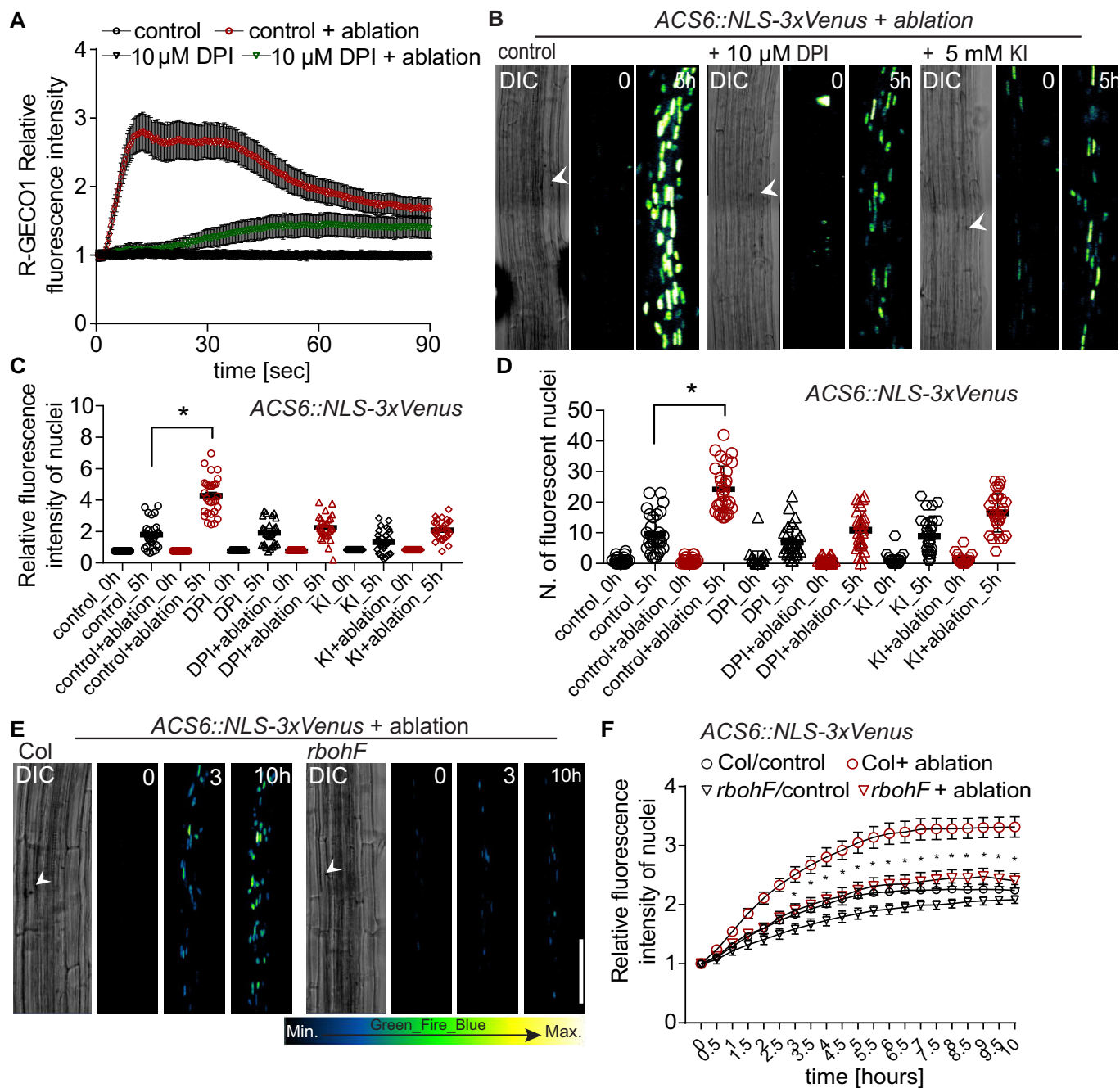


Figure 6. Laser ablation-induced calcium wave and ethylene biosynthesis require ROS production.

A Quantification of calcium wave propagation after cortex cell ablation using a *R-GECO1* reporter line (repeated two times, each with $n = 15$ roots; error bars indicate standard error). Application of ROS production inhibitor DPI (10 μM) significantly reduced calcium wave propagation after cortex cell ablation, when compared to ablated, non-treated controls.

B–D Visualization (**B**) and quantification (**C**, **D**) of *ACS6::NLS-3xVenus* after laser ablation on either control medium or with 10 μM DPI or 5 mM KI at time 0 and 5 h. (**B**) White arrowhead indicates position of ablated cell. (**C**, **D**) Number of cells with positive nuclear signal (**D**) and average signal intensities (**C**); increases observed 5 h after ablation are significantly reduced upon inhibitor treatment ($*P < 0.05$, the significance was determined by t-test, data pooled from three independent experiments with $n = 10$ roots each; error bars indicate mean value with 95% CI).

E, **F** Time-lapse images of tile-scan 4D (xyz) maximum projection images of *ACS6::NLS-3xVenus* ethylene-response marker line (**E**) and quantification (**F**) after laser ablation in wt (*col*) and in the *rbohF* mutant. Time points at the top right corner of each frame. Ablated *col* root responds much stronger to cortex cell ablation, when compared to *rbohF* (**E**). White arrowhead indicates position of ablated cell. Time-lapse images of representative movies are shown. (**F**) Quantification of *ACS6* increase in average signal intensity ($*P < 0.05$, data pooled from three independent experiments with $n = 10$ roots each; error bars indicate standard error).

Data information: Scale bar: (**B**, **E**) 100 μm.

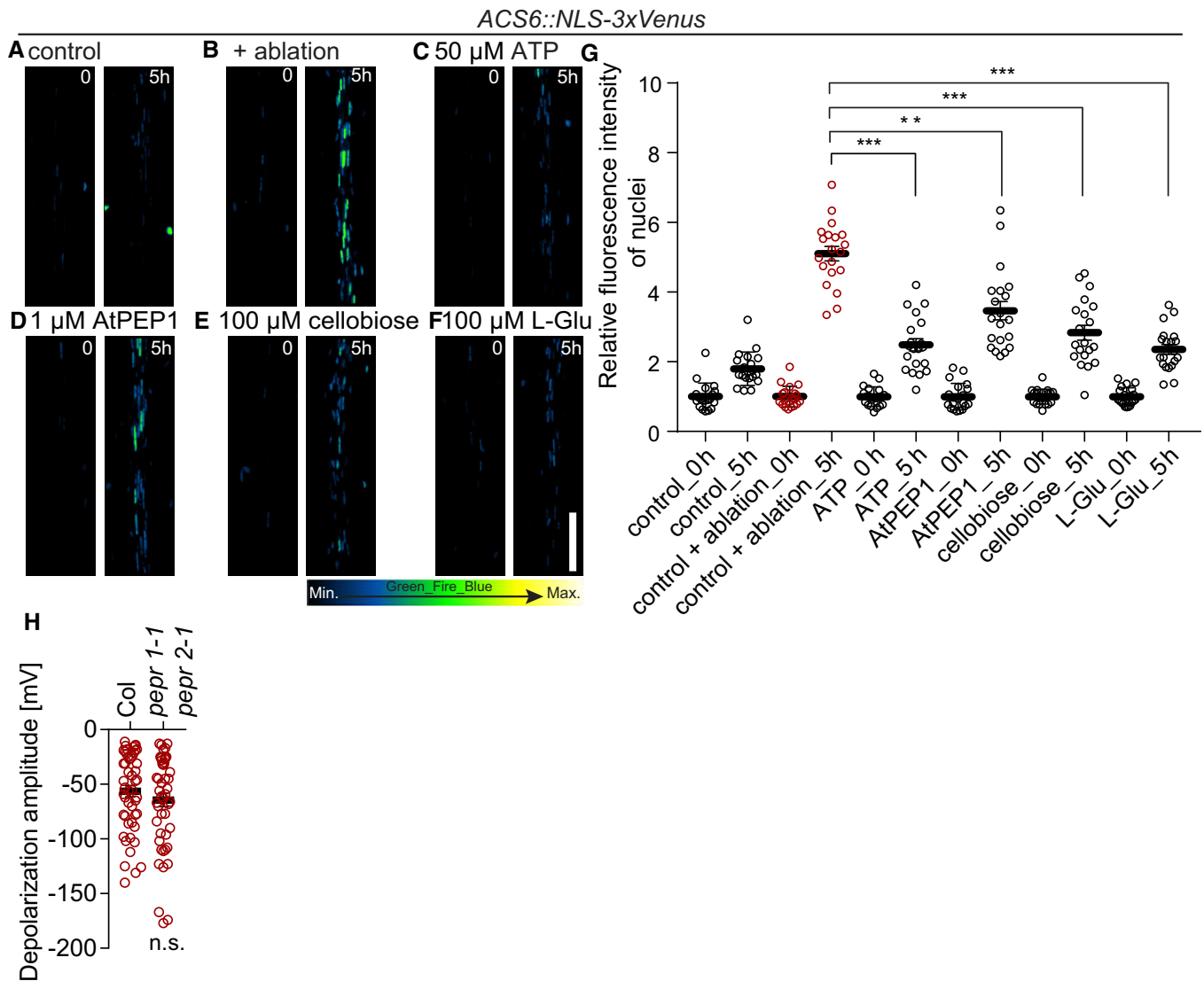


Figure 7. Induction of ACS6 by damage-associated molecular patterns.

A–F XYZ maximum projection images of *ACS6::NLS-3xVenus* ethylene biosynthesis marker after laser ablation (B) and upon treatment with ATP (50 μ M) (C), AtPEP1 (1 μ M) (D), cellobiose (100 μ M) (E), and L-glutamic acid (100 μ M) (F). Time points in seconds at the top right corner of each frame. Representative images are shown.

G Signal intensity quantification of *ACS6::NLS-3xVenus*. Signal intensity increases in all treatments, from time 0 h, but much less when compared to ablation ($***P < 0.0001$ and $**P < 0.001$, the significance was determined by *t*-test, data pooled from two independent experiments with $n = 10$ roots each; error bars indicate mean value with 95% CI).

H Quantification of depolarization amplitudes after cortex cell ablation were not reduced in *pepr1-1 pepr2-1* double mutant, compared to wt (Col) ($n = 30$ roots each; error bars indicate standard error; the significance was determined by *t*-test).

Data Information: Scale bar, (A–F) 100 μ m.

be generated in response to wounding, pathogen attack, or a local abiotic stress and be transmitted through the entire plant, often in an intricate, not fully understood, feedback loop with calcium (Miller *et al*, 2009). We investigated the contribution of ROS to the surface potential changes by analyzing *Arabidopsis* lines affected in ROS production by plasma membrane localized NADPH oxidases: *rbohA*, *rbohD*, *rbohF*, and *rbohDF* double mutants (Torres *et al*, 2002; Lee *et al*, 2013). We observed a reduced depolarization amplitude in *rbohD* and *F* mutants, but not in *rbohA* mutants (Fig 5A). In

line with the effects of the mutants, depolarization amplitude was also reduced by diphenyleneiodonium (DPI), an NAD(P)H oxidase inhibitor, as well as potassium iodide (KI), an H_2O_2 scavenger (Lee *et al*, 2013; Fig 5B). We visualized ROS production after laser ablation, by taking advantage of H_2DCFDA , a fluorescent indicator of ROS accumulation (Shin *et al*, 2005). After ablation, H_2DCFDA signals increased significantly in wild-type roots (Fig 5C–E; Appendix Fig S5F and G), while a much-reduced response was observed already in single *rboh* mutants, as well as double mutants

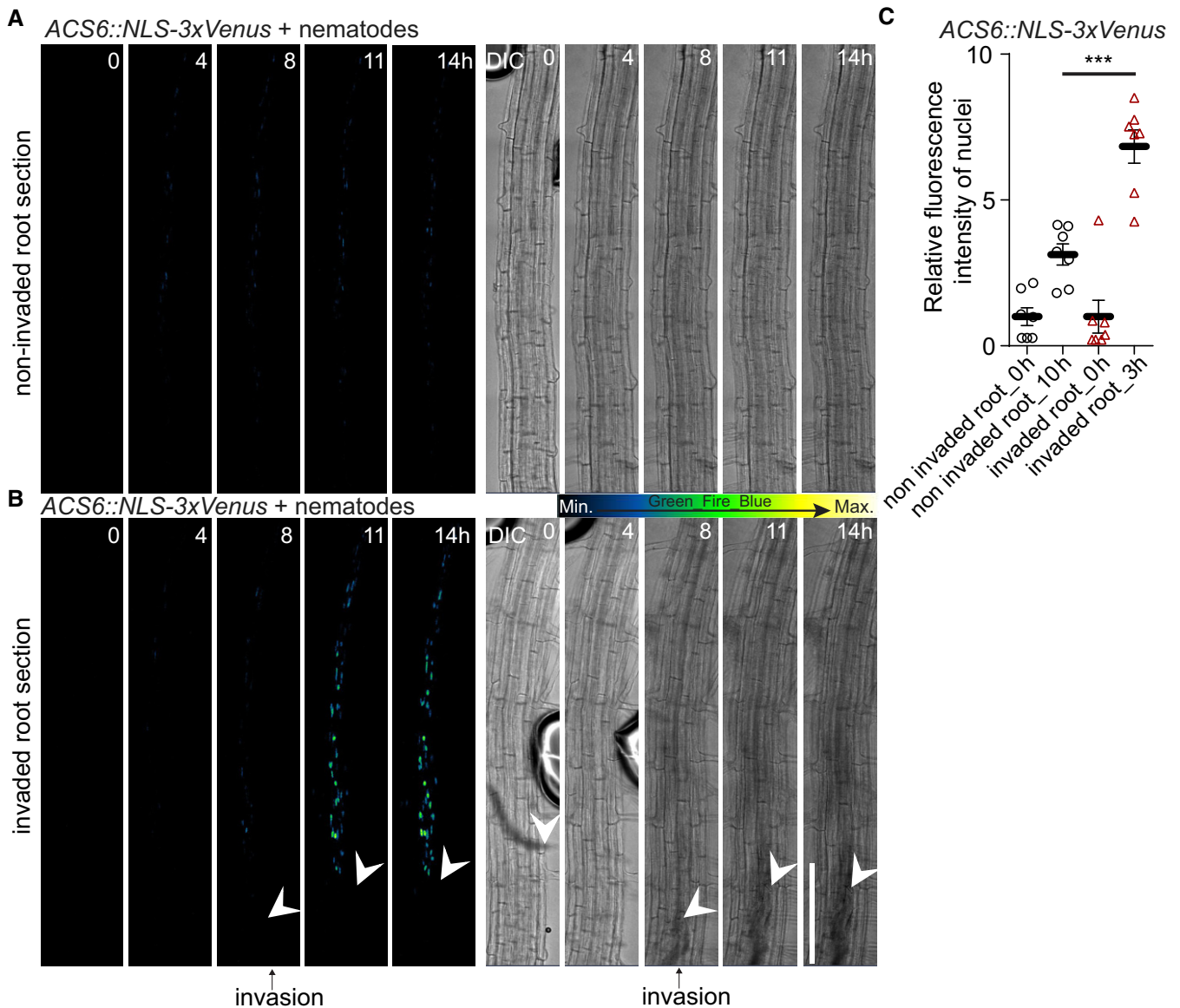


Figure 8. Cyst nematode damage leads to ethylene response.

A, B Tile-scan with 4D projection (xyz) images (A, B) monitoring ethylene biosynthesis by ACS6::NLS-3xVenus prior to cyst nematode (*Heterodera schachtii*) infection in 5-day-old roots. (A) Control scan demonstrating weak ACS6 response over 14 h in the non-invaded root section ($n = 9$). (B) ACS6 expression after nematode intrusion into root tissues ($n = 10$). White arrowheads indicate position of nematodes, and black arrows indicate time frame when nematode invasion of the root was first observed.

C ACS6::NLS-3xVenus ethylene biosynthesis marker line quantification 3 h after nematode intrusion into root tissues ($***P < 0.004$, the significance was determined by t-test; error bars indicate standard error, data pooled from three independent experiments).

Data information: Scale bar: (A, B) 100 μ m. See also Movies EV2–EV5.

(Fig 5E; Appendix Fig S5L–Q). DPI and KI treatment completely abrogated H₂DCFDA signals (Fig 5C and D; Appendix Fig S5H–K). Since calcium increases were only partially required for induction of ethylene production and response, we wondered whether ROS might be required. Indeed, the ablation-induced increases in calcium signals were blocked by DPI treatment (Fig 6A) and we could observe block in *pACS6* induction upon DPI and KI treatment (Fig 6B–D), as well as a decrease in *pACS6::NLS-3xVenus* signals in *rbohF* compared to wild-type roots (Fig 6E–F). Our data suggest that

laser ablation of single root cells induces a similar, albeit more localized, trio of depolarization, calcium influx, and ROS production, as is observed upon other stresses. However, in our case, both ROS production and calcium increases appear to feed into the induction of ethylene production and response.

The short IR-laser pulse causes loss of cellular integrity, which must lead to the release and/or generation of a great number of damage-associated molecular patterns (DAMPs), which could initiate the local ROS/calcium wave described here. However, even at

high concentrations, none of the known DAMPs tested (ATP, L-glutamic acid, cellobiose, AtPEP1) could induce *ACS6* expression to the same level than ablation of a single cortex cell (Fig 7A–G). Moreover, receptor mutants for AtPEP1 (and other AtPEPs) displayed the same degree of surface depolarization than the wild type (Fig 7H), indicating that putative DAMPs like AtPEP1 do not play a major role in initiating or transducing the regional depolarization upon ablation.

Cyst nematode attack induces surface potential changes and a protective ethylene response

Besides its role as a plant hormone regulating growth and development, ethylene has been known for decades to be induced upon various stresses (Yang & Hoffman, 1984) and to regulate the accumulation of specific defense genes (Ecker & Davis, 1987; Thomma *et al*, 1999), often in complex agonistic or antagonistic interaction with hormones such as jasmonate (Broekgaarden *et al*, 2015). We therefore hypothesized that the observed ethylene response might be protective against organisms that cause disruption of single cells during initial attack.

In nature, damage of single root cells could be caused by a variety of attackers, such as nematodes, small insect larvae, or invading necrotrophic microbes. Nematodes are omnipresent in soil, and thousands of plant parasitic species are known. During initial attack, many nematodes use their stylet to damage plant cells. Cyst nematodes (*Heterodera schachtii*) represent severe root pests and progress into roots by successively damaging single cells (Movies EV2 and EV3), making them an ideal model for our purpose (Holbein *et al*, 2016; Shah *et al*, 2017). We first investigated whether attacking cyst nematodes would generate surface potential changes similar to those observed during laser ablation. We measured surface potential changes before, during, and after nematode-mediated wounding (breaking of cells using the stylet) in combination with time-lapse confocal imaging. For controls, we placed the electrode on the root surface and simultaneously measured surface potential changes during confocal imaging in the absence of nematodes. In the control, the electrophysiological recording was stable and had a steady base level during the entire observation period (Appendix Fig S6C and D). However, when we placed cyst nematodes into the chamber with the seedlings, the recording revealed changes in depolarization amplitude (depolarization peaks) once the nematodes had

reached the root and started to cause tissue damage (Appendix Fig S6C and D). Long-term 4D confocal imaging (over a period of 14 h) of ethylene-response marker lines *pACS6::NLS-3xVenus* (Fig 8A–C; Movie EV4) and *pPR4::NLS-3xVenus* (Fig 9A–C; Movie EV5) during nematode attack revealed a strong increase in their expression at regions of nematode infection. Interestingly, corroborating our observations upon laser ablation—but in contradiction to earlier studies (Kammerhofer *et al*, 2015)—nematode invasion did not appear to induce a consistent jasmonate response, based on the lack of our *JAZ10::NLS-3xVenus* jasmonate reporter expression (Appendix Fig S7A–C). Nevertheless, our data clearly implicate ethylene in the response to localized mechanical injuries in roots and suggested that ethylene-induced genes might act to antagonize nematode infection. We therefore compared success of early stages of nematode infection between the wild type and two ethylene signaling mutants, measured by the time between root attack and initial syncytial cell (ISC) establishment. We found that interference with the ethylene pathway indeed increases nematode success rate, as measured by the faster establishment of the ISC stage in these mutants (Fig 9D), suggesting that the observed induction of ethylene production and response genes has a protective effect against nematodes. By contrast, neither jasmonate production nor signaling mutants (*aos* and *coi1*) affected nematode success in these early infection stages, consistent with the absent or very weak jasmonate response upon damage that we report here (Fig 9E). We also tested AtPEP1 receptor mutants (*pepr1 pepr2* double mutants) which also did not affect ISC establishment in our assays (Fig 9E).

Discussion

Many signaling molecules have been implicated in the wound responses of plants, and much research in the past decades has been focused on the trio of jasmonate, ethylene, and salicylic acid, which each elicits partially overlapping as well as distinct defense responses and which—depending on the nature of the attack, the plant species, or organ investigated—can have either antagonistic, independent, or synergistic activities (O'Donnell *et al*, 1996; Reymond & Farmer, 1998; Rojo *et al*, 1999; Lorenzo *et al*, 2003). Our transcriptional marker line data indicate that single-cell damage in roots causes a distinct, ethylene-dominated stress response, with no observable induction of jasmonate or salicylic acid. Jasmonate

Figure 9. Cyst nematode damage leads to ethylene response.

- A, B Time lapse of maximum projections of tile-scan XYZT images monitoring ethylene-response *PR4::NLS-3xVenus* prior to cyst nematode (*Heterodera schachtii*) infection in 5-day-old roots. (A) Absence of *PR4::NLS-3xVenus* response in a non-invaded root section over a 14-h nematode infection ($n = 10$). (B) *PR4::NLS-3xVenus* response to nematode intrusion into the root ($n = 7$). Time points at the top right corners. White arrows indicate nematode position inside the root (B), and the black arrow indicates the time frame when nematode invasion into the root was first observed.
- C *PR4::NLS-3xVenus* ethylene-response marker line quantification 3 h after nematode intrusion into root tissues (** $P < 0.003$, the significance was determined by *t*-test; error bars indicate standard error, data pooled from three independent experiments).
- D Analysis of success of root infection by nematodes, measuring the time of entering the root until establishment of initial syncytial cell (ISC). Nematodes invading ethylene signaling mutants *ein3-1* or *ein2-1* are significantly faster in establishing ISC than upon invasion of wt (Col) roots (** $P < 0.0005$, $n \geq 15$ nematodes, repeated three times; error bars indicate standard error).
- E Analysis of success of root infection by nematodes, measuring the time of entering the root until establishment of initial syncytial cell (ISC). Nematodes invading and establishing ISC upon invasion in wt (col) and the mutants *aos*, *coi1-34*, and *pepr1-1 pepr2-1* at the same timescale ($n \geq 20$ nematodes, pooled from three times repeated independent experiments; error bars indicate standard error; the significance was determined by *t*-test).

Data information: Scale bar: (A, B) 200 μm .

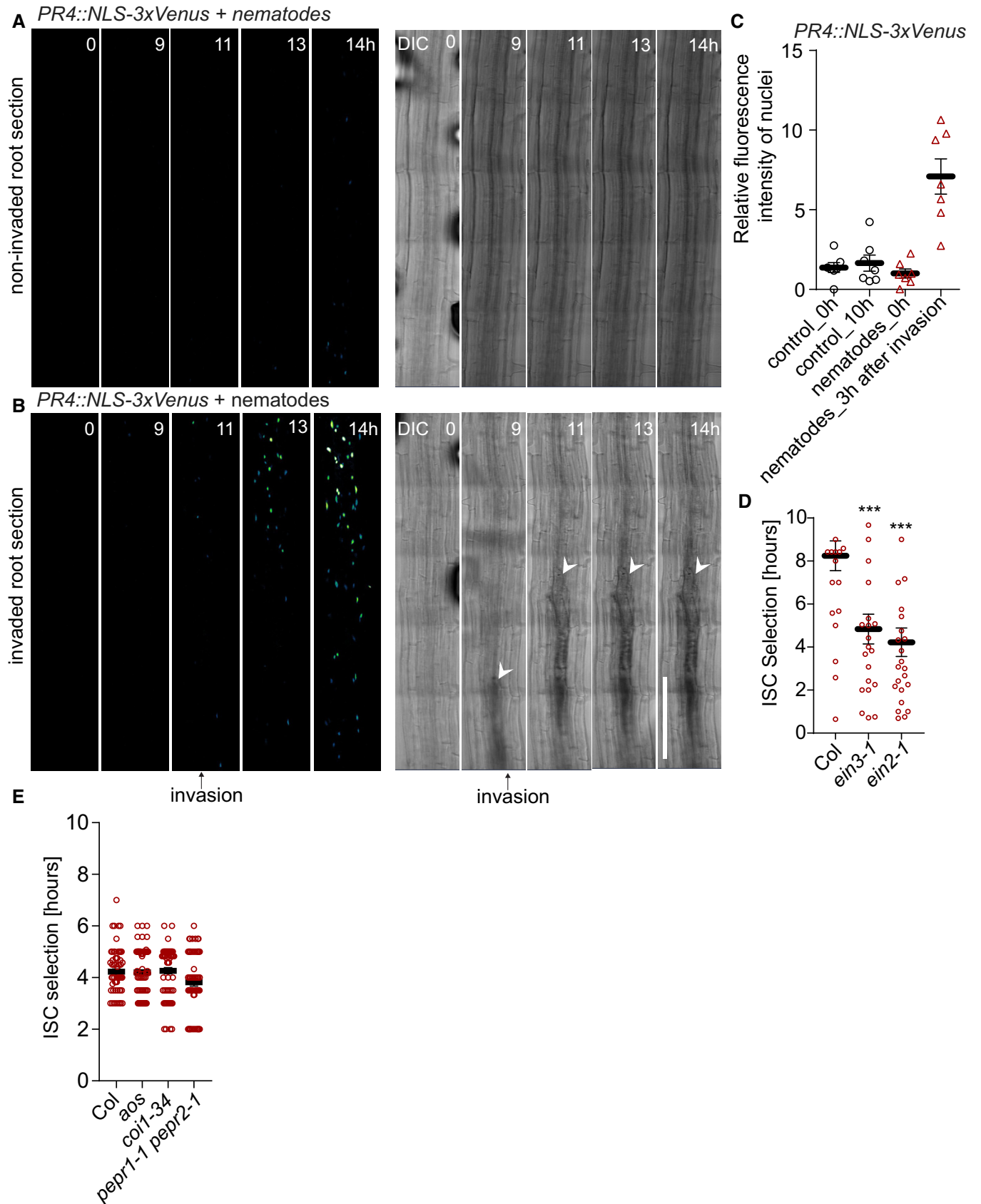


Figure 9.

generally appears to play a less predominant role in damage signaling of roots than of leaves, as similarly restricted, single-cell damage in cotyledons consistently induces expression of jasmonate reporters. Moreover, even more extensive damage of roots by crushing of root tips—or the progressive damage caused by nematodes—fails to induce a robust jasmonate response in our hands. This is consistent with a much weaker and more restricted expression of jasmonate biosynthesis LOX genes in roots (Gasperini *et al*, 2015a). Although earlier work did report modest inductions of jasmonate upon widespread crushing of mature root systems (Grebner *et al*, 2013), the difference might be explained by the very different age and growth conditions (6- to 8-week-old, hydroponically grown versus 5-day-old, agar-grown plants used herein). Old root systems, for example, have much more developed central veins and cambial activity, which might alter the way they respond to damage. Our results also do not contradict the important role of jasmonate in roots, both as a growth regulator and as a stress hormone (Vijayan *et al*, 1998; Chen *et al*, 2011; Denness *et al*, 2011; Carvalhais *et al*, 2015; Gasperini *et al*, 2015b), and jasmonate might have a more prominent role in meristematic root tissues. What our data indicate is that a conserved set of proximal events following damage (cytosolic calcium increase, ROS burst, depolarization) is not invariably linked to an increase in jasmonate production, but can instead be coupled to an exclusive, or predominant, production of ethylene.

Ethylene is a major regulator for a wide array of plant stresses, such as touch, wounding, or pathogen attack (Yang & Hoffman, 1984), and synthesis of 1-aminocyclopropane-1-carboxylate (ACC) by the ACC synthase (ACS) gene family has been shown genetically and biochemically to be a required and rate-limiting step in ethylene production (Zarembinski & Theologis, 1994; Li *et al*, 2012). Transcriptional induction of an ACS gene is therefore a good proxy for an increase in ethylene production. Upregulation of our ACS6 transcriptional reporter predominantly in the stele nevertheless does not exclude a more widespread induction of ethylene production, driven by ACS6 homologs, in cortical/epidermal tissues, for example. ACS6 transcriptional induction has been shown to require MAP kinases 3 and 6 (Li *et al*, 2012). Our observed regional increases in ROS and calcium could cause activation of MAP kinases. Alternatively, they might simply be associated events. This is the case for MAMP signaling, for example, where ROS production and cytosolic calcium increases on the one hand and MAP kinase activation on the other are seen as parallel events downstream of receptor activation.

A catastrophic collapse of cellular integrity of a single cell, as induced by laser, nematode stylet, or other physical stresses, should cause a highly localized release and generation of a complex cocktail of DAMPs, but also massive amounts of vacuolar solutes, proteases, and other enzymes. In addition, it should generate mechanical stresses on neighboring cells. We speculate that a complex combination of these factors is required for effective signaling of cellular damage to the surrounding cells.

The regional, wound-induced depolarization that we observe appears to depend on a number of transporter and channel activities that are known to regulate and maintain plant transmembrane potentials. We did not resolve whether any of the implicated activities, such as proton pumps or potassium, chloride, or calcium channels, are directly involved in cell-to-cell signal propagation or are

simply affecting the transmembrane potential of the epidermal cells proximal to the electrode, for example. It is intriguing that mutations in specific NADPH oxidases affected surface depolarization after wounding, since a causal connection between wound-induced ROS production and membrane depolarization in plants has not been established to our knowledge. Again, apoplastic ROS production could be involved in signal propagation, by activating calcium or other channels, for example, as is proposed in calcium/ROS wave propagation models (Gilroy *et al*, 2016). Alternatively, the electron transfer associated with NADPH oxidase-dependent ROS production might directly cause the membrane depolarizations we observe. Electron transfer from intracellular NADPH to extracellular oxygen by NADPH oxidases has been shown to generate plasma membrane currents in animal cells (Schrenzel *et al*, 1998). However, little attention has been paid to such a possible role of NADPH oxidases in transmembrane depolarization in plants. A possible scenario is that the electrogenic activity of RBOHF and RBOHD participates directly in the production of the damage-induced electrical signals we detected. The associated release of H⁺ from NADPH at the intracellular membrane face may additionally affect membrane potential (e.g., Demaurex & Petheö, 2005). RBOH-controlled changes in membrane potential could, in theory, also cause increases in cytosolic calcium levels.

Proton and electron generation/movement might therefore contribute directly to plasma membrane depolarization in response to insults such as nematode attack.

Our observation that nematode ISC stage establishment is affected by ethylene, but not jasmonate signaling, nicely corroborates our laser ablation data and points to the biological relevance of our findings. The results are only seemingly at odds with earlier studies demonstrating induction and functional relevance of jasmonate during nematode infection. Assays of nematode infection that assess overall success of nematodes by comparing female-to-male ratio inevitably confound the role of hormones at many different stages of infection, such as attraction, initial attack, migration, feeding site establishment, and reproduction. Each of these stages might be promoted or hindered by jasmonate, ethylene, or connected hormone signaling pathways. Our study, by contrast, has focused on monitoring and measuring nematode success in the window where cellular damage is caused, i.e., from the first root contact to the initial establishment of a feeding structure. This minimizes confounding effects of other hormones from different stages of infection. Indeed, most jasmonate responses described during cyst nematode infection are during later, syncytium stages, with one study reporting that they contribute to susceptibility, not resistance (Ozalvo *et al*, 2014). A weak upregulation of jasmonate responses observed in a microarray was again at a stage when nematodes could have reached the syncytial stage of development already (Kammerhofer *et al*, 2015). We therefore propose that the role of jasmonate during nematode infection is not associated with cellular damage, but rather with some of the many other developmental or defense-related roles described for jasmonate (Wasternack, 2014). We believe that our analysis of single-cell damage fills an important gap in our current understanding of mechanical stress responses, between cell-autonomous, touch-induced responses (Monshausen *et al*, 2009) and the systemic signals induced by macroscopic organ damage (Mousavi *et al*, 2013; Toyota *et al*, 2018). Single-cell laser ablations in roots indeed represent a powerful proxy for analyzing

early events of attacks by small invaders such as nematodes. More generally, single-cell ablations might be a valuable addition to studies of plant wound and defense responses, as they do not confound the potentially distinct responses of many different cell types that might display differences in quality, amplitude, and timing. This could be of a great advantage for the investigation of the immediate molecular and cellular mechanisms underlying damage perception in plants.

Materials and Methods

Plant material

Transgenic *Arabidopsis thaliana* (L.) Heynh. lines have been described elsewhere: Col; *rboh A* (GABI_397C02), *rboh F* (At1G64060), *rboh D* (SALK_070610) (Lee et al, 2013); *rboh DF* (Torres et al, 2002); *ein2-1* (Guzmán & Ecker, 1990); *ein3-1* (Chao et al, 1997); *pepr1-1 pepr2-1* (Yamaguchi et al, 2010); *glr3.3 3.1*, *glr3.3 3.6* (Nguyen et al, 2018); *aos* (Park et al, 2002); *coi1-34* (Acosta et al, 2013); *LOX6::LOX6-GUS* (Gasparini et al, 2015a,b); *35S::JAS9-Venus* (Larrieu et al, 2015); R-GECO1 (Keinath et al, 2015); Case12 (Matzke & Matzke, 2015); and *pPR1::NLS3xVenus* (Poncini et al, 2017). Generation of: *pACS6::NLS3xVenus* and *pPR4::NLS3xVenus*; *pJAZ10::NLS3xVenus*, *pAOS::NLS3xVenus*. The vector pGreenII229NLS3xmVenus containing the coding sequence for the mVenus reporter with a nuclear localization signal was from Vermeer et al (2014). The promoter regions of *JAZ10* (At5g13220), *ACS6* (At4g11280), *AOS* (At5g42650), and *HEL/PR4* (At3g04720) were amplified by PCR from genomic DNA of Col and cloned into the KpnI site of pGreenII229NLS3xmVenus. The constructs obtained (referred to as *promoter::mVenus*) were used to transform *Arabidopsis thaliana* ecotype Col-0 using *Agrobacterium tumefaciens* (GV3101) and selected with BASTA.

The primer sequences used for constructing entry clones were as follows:

pACS6::NLS3xVenus
 Fwd 5' ATTTGGTACCATGTCAACTAAAACCG 3'
 Rvs 5' AAGCGGTACCTTTTTGTTCTTCTTTA 3''
pPR4::NLS3xVenus
 Fwd 5' TAAGGTACCTAAATGACATGAGATG 3'
 Rvs 5' TGATGGTACCGATCGATAAGTCTTTG 3'
pJAZ10::NLS3xVenus
 Fwd 5'AAAAAGGTACCGGAGCAAACCTTACGCAA 3'
 Rvs 5'AAAAAGGTACCATCAAGACAGAGATATGGG 3'
pAOS::NLS3xVenus
 Fwd 5'AAAAAGGTACCGAAAAGCTTACC 3'
 Rvs 5'AAAAAGGTACCTATTCGAAACAGTGGCGAGT 3'.

Growth conditions

Seeds of *Arabidopsis* (accession Columbia-0) were placed on 1/2 MS (Murashige and Skoog) agar plates. The seeds were stratified for 2 days at 4°C. Seedlings were grown on vertically oriented plates in Percival growth chambers at 22°C under a 16-h light/8-h dark photoperiod at 21°C. Nematodes were cultured in Knop's nutrient medium under previously described conditions (Siddique et al, 2014).

Pharmacological and hormonal treatments

Five-day-old seedlings were transferred onto solid MS media containing 1% agar with or without the indicated chemicals and incubated during imaging and/or surface potential measurements. For electrophysiology experiments, 30-min pretreatments with inhibitor were performed on solid MS medium. Drugs and hormones used were as follows: tetraethylammonium (TEA; 50 μM), diphenylethylidonium (DPI; 10 μM), potassium iodide (KI; 5 mM), anthracene-9-carboxylic acid (A9C; 50 μM), methoxyverapamil (50 μM), gadolinium chloride (GdCl₃; 50 μM), vanadium (50 μM), N,N'-dicyclohexylcarbodiimide (DCCD; 50 μM), adenosine triphosphate (ATP; 50 μM), activator of plant plasma membrane proton pumps (fusicoicin; 5 μM), plant elicitor peptide (PEP1; 1 μM), cellobiose (100 μM), L-glutamate (100 μM), 1-aminocyclopropanecarboxylic acid (ACC; 2 μM), methyl jasmonate (MeJA; 1 μM), and salicylic acid (SA; 1 μM). Fluorescent dyes used were as follows: propidium iodide (PI; 10 mg/μl) and 2',7'-dichlorodihydrofluorescein diacetate (H₂DCFDA; 20 μM). Five-day-old seedlings were placed onto solid medium containing PI or H₂DCFDA and immediately imaged during entire short/long period of experiments.

Histochemical staining for GUS activity and ClearSee protocols

LOX6::LOX6-GUS – expressing in 5-day-old seedlings before/after manual crushing of roots were stained for GUS activity (promoter-driven GUS, beta-glucuronidase) as described (Benková et al, 2003). Immediately after stopping the GUS reaction, seedlings were placed in a ClearSee solution as described in Kurihara et al (2015) and Ursache et al (2018) and incubated for 3 days. After 3 days, the ClearSee solution was replaced with ClearSee solution combining calcofluor white for 2 h (Ursache et al, 2018) and imaged by Zeiss LSM 880 inverted confocal scanning microscope.

Confocal imaging and real-time analysis

For confocal microscopy images, the Zeiss LSM 880 inverted confocal scanning microscope was used. Pictures were taken with 10× and 40× water immersion objectives. For more detailed analyses, imaging was performed with Z-scans plus tile-scans (overlap 15%). Fluorescence signals for green fluorescent protein (GFP) (excitation 488 nm, emission 500–530 nm), for yellow fluorescent protein the GFP settings were used; propidium iodide (excitation 520 nm, emission 590 nm), calcofluor white (excitation 405 nm, emission 415–443 nm) and for the GUS (excitation Alexa Fluor 488—T80/R20), were detected. Sequential scanning was used to avoid any interference between fluorescence channels. The sample preparation and manipulation for short and long-term imaging was described previously (Marhavý et al, 2014; Marhavý & Benková, 2015). For time lapse (long-term imaging), the roots were scanned in 1-, 10-, 20-, or 30-min intervals for 10–24 h. For image analyses, the ImageJ (NIH; <http://rsb.info.nih.gov/ij>) and Zeiss Zen (black edition) software packages were used. The statistical significance was evaluated with Student's *t*-test.

Laser ablation

Cell ablation experiments were performed with a Zeiss LSM 880 Confocal/Multiphoton microscope (Mai Tai Spectra-Physics

Multiphoton laser). For ablation, we used a 40× water immersion objective, scaling dimensions (xyz), laser (800 nm) setting 2%, beam splitter MBS_InVis: MBS 760+, and pixel dwell 0.8 μs. ROIs were drawn through cells prior to ablation.

Ca²⁺ wave velocity analyses

Cortical and epidermal localizations of Ca²⁺ wave increase monitored 100 μm from ablation side within the cortex or epidermal cell file. Images were recorded every 0.3 s.

Surface potential recordings

For surface potential recordings, silver electrodes 0.1 mm in diameter (World Precision Instruments) were chloridized with HCl (0.1 M). Experiments were conducted in the Faraday cage simultaneously with confocal microscopy. A dual-channel differential electrometer (FD 223a; World Precision Instruments) under the control of LabScribe2 software (World Precision Instruments) was used to record signal. The signal acquisition interval was 0.01 s. Electrodes were placed on the root epidermis in positions distal to ablations with the use of M3301R manual micromanipulators (World Precision Instruments). The ground electrode was placed in the 1/2 MS solid medium away from the two-photon laser range in the same chamber, where the seedlings were placed. Surface potential amplitudes were calculated in relation to the baseline before ablation.

Nematodes

We used cyst nematodes, *Heterodera schachtii*. The incubation and manipulation of cyst nematodes, *Heterodera schachtii*, was done as described previously (Siddique *et al*, 2014).

Nematodes microscopy

Five-day-old seedlings were placed in Nunc Lab-Tek Chambers as described in Marhavý *et al* (2014, 2016), and Marhavý and Benková (2015). On top of the solid media that covered roots, a 50-μl drop of liquid media containing 40 ± 5 nematodes was added with immediate imaging and/or surface potential measurements. During long-term time-lapse imaging, nematodes invade the roots with 90–100% success rate. Due to unpredictable nematode invasion of the root region, the success rate of observation during invasion was ± 50%.

ISC establishment assays

Arabidopsis plants were grown on Knop's medium, and 12-day-old plants were inoculated with *Heterodera schachtii* as described previously (Siddique *et al*, 2014). For ISC establishment assays, the positions of cyst nematode larvae that entered the epidermis were marked with permanent markers on the Petri dishes. Afterward, nematodes and their stylet movements were observed every 30 min. Initial syncytial cell establishment was defined as the cessation of nematode and stylet movements. Three biological replicates were performed and 15–25 nematodes were observed for each genotype per single biological replicate.

Software used

For image analyses and video processing/editing, ImageJ (NIH; <http://rsb.info.nih.gov/ij>) and Zeiss Zen2.1 (black edition) software packages were used. For electrophysiology recording and data analysis, LabScribe2 (World Precision Instruments) software was used. Graphs were generated in Microsoft Excel or in GraphPad Prism 7.04. Figures were organized in Adobe Illustrator CC 2018.

Expanded View for this article is available online.

Acknowledgements

We thank Tom Beeckman, Dolf Weijers, Bruno Müller, and Martin Heil for helpful discussions, Antonius Matzke for sharing published material, and Yong-Qiang Gao for help with electrical circuit measurements. This work was supported by funds to N.G. from an ERC Consolidator Grant (GA-No.: 616228—ENDOFUN), two SNSF grants (CRSII3_136278 and 31003A_156261), a DFG grant to S.S. (SI 1739/3-1), a Federation of European Biochemical Sciences Long-Term Postdoctoral Fellowship to P.M., and an EMBO Long-Term Postdoctoral Fellowship to F.Z.

Author contributions

PM initiated, planned, and conceived the project with input from NG and EEF; PM, AK, SS, FZ, JH, VDT, and MSH carried out the experiments; and FMWG edited the manuscript. All authors discussed the project. PM and NG wrote the manuscript, and all authors read and provided comments to the manuscript.

Conflict of interest

The authors declare that they have no conflict of interest.

References

- Acosta IF, Gasperini D, Chételat A, Stolz S, Santuari L, Farmer EE (2013) Role of NINJA in root jasmonate signaling. *Proc Natl Acad Sci USA* 110: 15473–15478
- Albrecht V, Weinl S, Blazevic D, D'Angelo C, Batistic O, Kolukisaoglu U, Bock R, Schulz B, Harter K, Kudla J (2003) The calcium sensor CBL1 integrates plant responses to abiotic stresses. *Plant J Cell Mol Biol* 36: 457–470
- Benfey PN, Scheres B (2000) Root development. *Curr Biol* 10: R813–R815
- Benková E, Michniewicz M, Sauer M, Teichmann T, Seifertová D, Jürgens G, Friml J (2003) Local, efflux-dependent auxin gradients as a common module for plant organ formation. *Cell* 115: 591–602
- van den Berg C, Willemsen V, Hendriks G, Weisbeek P, Scheres B (1997) Short-range control of cell differentiation in the *Arabidopsis* root meristem. *Nature* 390: 287–289
- Broekgaarden C, Caarls L, Vos IA, Pieterse CMJ, Wees SCMV (2015) Ethylene: traffic controller on hormonal crossroads to defense. *Plant Physiol* 169: 2371–2379
- Carvalhais LC, Dennis PG, Badri DV, Kidd BN, Vivanco JM, Schenk PM (2015) Linking jasmonic acid signaling, root exudates, and rhizosphere microbiomes. *Mol Plant Microbe Interact* 28: 1049–1058
- Catterall WA, Wisedchaisri G, Zheng N (2017) The chemical basis for electrical signaling. *Nat Chem Biol* 13: 455–463
- Chao Q, Rothenberg M, Solano R, Roman G, Terzaghi W, Ecker JR (1997) Activation of the ethylene gas response pathway in *Arabidopsis* by the

- nuclear protein ETHYLENE-INSENSITIVE3 and related proteins. *Cell* 89: 1133–1144
- Chen Q, Sun J, Zhai Q, Zhou W, Qi L, Xu L, Wang B, Chen R, Jiang H, Qi J et al (2011) The basic helix-loop-helix transcription factor MYC2 directly represses PLETHORA expression during jasmonate-mediated modulation of the root stem cell niche in *Arabidopsis*. *Plant Cell* 23: 3335–3352
- Choi J, Tanaka K, Cao Y, Qi Y, Qiu J, Liang Y, Lee SY, Stacey G (2014) Identification of a plant receptor for extracellular ATP. *Science* 343: 290–294
- Choi WG, Hilleary R, Swanson SJ, Kim S-H, Gilroy S (2016) Rapid, long-distance electrical and calcium signaling in plants. *Annu Rev Plant Biol* 67: 287–307
- Demaurex N, Petheö GL (2005) Electron and proton transport by NADPH oxidases. *Philos Trans R Soc Lond B Biol Sci* 360: 2315–2325
- Denness L, McKenna JF, Segonzac C, Wormit A, Madhou P, Bennett M, Mansfield J, Zipfel C, Hamann T (2011) Cell wall damage-induced lignin biosynthesis is regulated by a reactive oxygen species- and jasmonic acid-dependent process in *Arabidopsis*. *Plant Physiol* 156: 1364–1374
- Duran-Flores D, Heil M (2016) Sources of specificity in plant damaged-self recognition. *Curr Opin Plant Biol* 32: 77–87
- Ecker JR, Davis RW (1987) Plant defense genes are regulated by ethylene. *Proc Natl Acad Sci USA* 84: 5202–5206
- Flucher BE, Tuluc P (2017) How and why are calcium currents curtailed in the skeletal muscle voltage-gated calcium channels? *J Physiol* 595: 1451–1463
- Gasparini D, Chauvin A, Acosta IF, Kurenda A, Stolz S, Chételat A, Wolfender J-L, Farmer EE (2015a) Axial and radial oxylipin transport. *Plant Physiol* 169: 2244–2254
- Gasparini D, Chételat A, Acosta IF, Goossens J, Pauwels L, Goossens A, Dreos R, Alfonso E, Farmer EE (2015b) Multilayered organization of jasmonate signalling in the regulation of root growth. *PLoS Genet* 11: e1005300
- Gilroy S, Suzuki N, Miller G, Choi W-G, Toyota M, Devireddy AR, Mittler R (2014) A tidal wave of signals: calcium and ROS at the forefront of rapid systemic signaling. *Trends Plant Sci* 19: 623–630
- Gilroy S, Białasek M, Suzuki N, Górecka M, Devireddy AR, Karpinski S, Mittler R (2016) ROS, calcium, and electric signals: key mediators of rapid systemic signaling in Plants1[OPEN]. *Plant Physiol* 171: 1606–1615
- Grebner W, Stingl NE, Oenel A, Mueller MJ, Berger S (2013) Lipoxygenase6-dependent oxylipin synthesis in roots is required for abiotic and biotic stress resistance of *Arabidopsis*. *Plant Physiol* 161: 2159–2170
- Guzmán P, Ecker JR (1990) Exploiting the triple response of *Arabidopsis* to identify ethylene-related mutants. *Plant Cell* 2: 513–523
- Hacquard S, Spaepen S, Garrido-Oter R, Schulze-Lefert P (2017) Interplay between innate immunity and the plant microbiota. *Annu Rev Phytopathol* 55: 565–589
- Holbein J, Grundler FMW, Siddique S (2016) Plant basal resistance to nematodes: an update. *J Exp Bot* 67: 2049–2061
- Kammerhofer N, Radakovic Z, Regis JMA, Dobrev P, Vankova R, Grundler FMW, Siddique S, Hofmann J, Wiczorek K (2015) Role of stress-related hormones in plant defence during early infection of the cyst nematode *Heterodera schachtii* in *Arabidopsis*. *New Phytol* 207: 778–789
- Keinath NF, Waadt R, Brugman R, Schroeder JI, Grossmann G, Schumacher K, Krebs M (2015) Live cell imaging with R-GECO1 sheds light on flg22- and chitin-induced transient [Ca²⁺]_{cyt} patterns in *Arabidopsis*. *Mol Plant* 8: 1188–1200
- Kinraide TB (2006) Plasma membrane surface potential (psiPM) as a determinant of ion bioavailability: a critical analysis of new and published toxicological studies and a simplified method for the computation of plant psiPM. *Environ Toxicol Chem* 25: 3188–3198
- Kurihara D, Mizuta Y, Sato Y, Higashiyama T (2015) ClearSee: a rapid optical clearing reagent for whole-plant fluorescence imaging. *Development* 142: 4168–4179
- Laureau A, Champion A, Legrand J, Lavenus J, Mast D, Brunoud G, Oh J, Guyomarc'h S, Pizot M, Farmer EE et al (2015) A fluorescent hormone biosensor reveals the dynamics of jasmonate signalling in plants. *Nat Commun* 6: 6043
- Lee Y, Rubio MC, Allassimone J, Geldner N (2013) A mechanism for localized lignin deposition in the endodermis. *Cell* 153: 402–412
- Li G, Meng X, Wang R, Mao G, Han L, Liu Y, Zhang S (2012) Dual-level regulation of ACC synthase activity by MPK3/MPK6 cascade and its downstream WRKY transcription factor during ethylene induction in *Arabidopsis*. *PLoS Genet* 8: e1002767
- Lim JH, Oh EH, Park J, Hong S, Park TH (2015) Ion-channel-coupled receptor-based platform for a real-time measurement of G-protein-coupled receptor activities. *ACS Nano* 9: 1699–1706
- Liu Y, Zhang S (2004) Phosphorylation of 1-aminocyclopropane-1-carboxylic acid synthase by MPK6, a stress-responsive mitogen-activated protein kinase, induces ethylene biosynthesis in *Arabidopsis*. *Plant Cell* 16: 3386–3399
- Lorenzo O, Piqueras R, Sánchez-Serrano JJ, Solano R (2003) ETHYLENE RESPONSE FACTOR1 integrates signals from ethylene and jasmonate pathways in plant defense. *Plant Cell* 15: 165–178
- Marhavý P, Duclercq J, Weller B, Feraru E, Bielach A, Offringa R, Friml J, Schwechheimer C, Murphy A, Benková E (2014) Cytokinin controls polarity of PIN1-dependent auxin transport during lateral root organogenesis. *Curr Biol* 24: 1031–1037
- Marhavý P, Benková E (2015) Real-time analysis of lateral root organogenesis in *Arabidopsis*. *Bio Protoc* 5: e1446
- Marhavý P, Montesinos JC, Abuzeineh A, Van Damme D, Vermeer JEM, Duclercq J, Rakusová H, Nováková P, Friml J, Geldner N et al (2016) Targeted cell elimination reveals an auxin-guided biphasic mode of lateral root initiation. *Genes Dev* 30: 471–483
- Matzke AJM, Matzke M (2015) Expression and testing in plants of ArcLight, a genetically-encoded voltage indicator used in neuroscience research. *BMC Plant Biol* 15: 245
- Miller G, Schlauch K, Tam R, Cortes D, Torres MA, Shulaev V, Dangl JL, Mittler R (2009) The plant NADPH oxidase RBOHD mediates rapid systemic signaling in response to diverse stimuli. *Sci Signal* 2: ra45
- Mishra B, Carson R, Hume RI, Collins CA (2013) Sodium and potassium currents influence Wallerian degeneration of injured *Drosophila* axons. *J Neurosci* 33: 18728–18739
- Monshausen GB, Messerli MA, Gilroy S (2008) Imaging of the Yellow Cameleon 3.6 indicator reveals that elevations in cytosolic Ca²⁺ follow oscillating increases in growth in root hairs of *Arabidopsis*. *Plant Physiol* 147: 1690–1698
- Monshausen GB, Bibikova TN, Weissenfeldt MH, Gilroy S (2009) Ca²⁺ regulates reactive oxygen species production and pH during mechanosensing in *Arabidopsis* roots. *Plant Cell* 21: 2341–2356
- Mousavi SAR, Chauvin A, Pascaud F, Kellenberger S, Farmer EE (2013) GLUTAMATE RECEPTOR-LIKE genes mediate leaf-to-leaf wound signalling. *Nature* 500: 422–426
- Nguyen CT, Kurenda A, Stolz S, Chételat A, Farmer EE (2018) Identification of cell populations necessary for leaf-to-leaf electrical signaling in a wounded plant. *Proc Natl Acad Sci* 115: 10178–10183
- O'Donnell PJ, Calvert C, Atzorn R, Wasternack C, Leyser HMO, Bowles DJ (1996) Ethylene as a signal mediating the wound response of tomato plants. *Science* 274: 1914–1917

- Ozalvo R, Cabrera J, Escobar C, Christensen SA, Borrego EJ, Kolomiets MV, Castresana C, Iberkleid I, Brown Horowitz S (2014) Two closely related members of *Arabidopsis* 13-lipoxygenases (13-LOXs), LOX3 and LOX4, reveal distinct functions in response to plant-parasitic nematode infection. *Mol Plant Pathol* 15: 319–332
- Pandey GK, Cheong YH, Kim K-N, Grant JJ, Li L, Hung W, D'Angelo C, Weinl S, Kudla J, Luan S (2004) The calcium sensor calcineurin B-like 9 modulates abscisic acid sensitivity and biosynthesis in *Arabidopsis*. *Plant Cell* 16: 1912–1924
- Park J-H, Halitschke R, Kim HB, Baldwin IT, Feldmann KA, Feyereisen R (2002) A knock-out mutation in allene oxide synthase results in male sterility and defective wound signal transduction in *Arabidopsis* due to a block in jasmonic acid biosynthesis. *Plant J Cell Mol Biol* 31: 1–12
- Perez Garcia MT, Ciudad P, Lopez-Lopez JR (2017) The secret life of ion channels: Kv1.3 potassium channels and cell proliferation. *Am J Physiol Cell Physiol* 314: C27–C42
- Pickard BG, Ding JP (1993) The mechanosensory calcium-selective ion channel: key component of a plasmalemmal control centre? *Aust J Plant Physiol* 20: 439–459
- Poncini L, Wyrsh I, Déneraud Tendon V, Vorley T, Boller T, Geldner N, Métraux J-P, Lehmann S (2017) In roots of *Arabidopsis thaliana*, the damage-associated molecular pattern AtPep1 is a stronger elicitor of immune signalling than flg22 or the chitin heptamer. *PLoS One* 12: e0185808
- Proietti S, Bertini L, Van der Ent S, Leon-Reyes A, Pieterse CMJ, Tucci M, Caporale C, Caruso C (2011) Cross activity of orthologous WRKY transcription factors in wheat and *Arabidopsis*. *J Exp Bot* 62: 1975–1990
- Reymond P, Farmer EE (1998) Jasmonate and salicylate as global signals for defense gene expression. *Curr Opin Plant Biol* 1: 404–411
- Rojo E, León J, Sánchez-Serrano JJ (1999) Cross-talk between wound signalling pathways determines local versus systemic gene expression in *Arabidopsis thaliana*. *Plant J Cell Mol Biol* 20: 135–142
- Schrenzel J, Serrander L, Bánfi B, Nüsse O, Fouyouzi R, Lew DP, Demareux N, Krause KH (1998) Electron currents generated by the human phagocyte NADPH oxidase. *Nature* 392: 734–737
- Shah SJ, Anjam MS, Mendy B, Anwer MA, Habash SS, Lozano-Torres JL, Grundler FMW, Siddique S (2017) Damage-associated responses of the host contribute to defence against cyst nematodes but not root-knot nematodes. *J Exp Bot* 68: 5949–5960
- Shin R, Berg RH, Schachtman DP (2005) Reactive oxygen species and root hairs in *Arabidopsis* root response to nitrogen, phosphorus and potassium deficiency. *Plant Cell Physiol* 46: 1350–1357
- Shomer I, Novacky AJ, Pike SM, Yermiyahu U, Kinraide TB (2003) Electrical potentials of plant cell walls in response to the ionic environment. *Plant Physiol* 133: 411–422
- Siddique S, Matera C, Radakovic ZS, Hasan MS, Gutbrod P, Rozanska E, Sobczak M, Torres MA, Grundler FMW (2014) Parasitic worms stimulate host NADPH oxidases to produce reactive oxygen species that limit plant cell death and promote infection. *Sci Signal* 7: ra33
- Steinhorst L, Kudla J (2014) Signaling in cells and organisms – calcium holds the line. *Curr Opin Plant Biol* 22: 14–21
- Thomma BPHJ, Eggermont K, Tierens KFM-J, Broekaert WF (1999) Requirement of functional ethylene-insensitive 2 gene for efficient resistance of *Arabidopsis* to infection by *Botrytis cinerea*. *Plant Physiol* 121: 1093–1101
- Torres MA, Dangl JL, Jones JDG (2002) *Arabidopsis* gp91phox homologues AtrbohD and AtrbohF are required for accumulation of reactive oxygen intermediates in the plant defense response. *Proc Natl Acad Sci USA* 99: 517–522
- Toyota M, Spencer D, Sawai-Toyota S, Jiaqi W, Zhang T, Koo AJ, Howe GA, Gilroy S (2018) Glutamate triggers long-distance, calcium-based plant defense signaling. *Science* 361: 1112–1115
- Tsuchisaka A, Theologis A (2004) Unique and overlapping expression patterns among the *Arabidopsis* 1-amino-cyclopropane-1-carboxylate synthase gene family members. *Plant Physiol* 136: 2982–3000
- Ursache R, Andersen TG, Marhávy P, Geldner N (2018) A protocol for combining fluorescent proteins with histological stains for diverse cell wall components. *Plant J Cell Mol Biol* 93: 399–412
- Vermeer JEM, von Wangenheim D, Barberon M, Lee Y, Stelzer EHK, Maizel A, Geldner N (2014) A spatial accommodation by neighboring cells is required for organ initiation in *Arabidopsis*. *Science* 343: 178–183
- Véry AA, Sentenac H (2002) Cation channels in the *Arabidopsis* plasma membrane. *Trends Plant Sci* 7: 168–175
- Vijayan P, Shockey J, Lévesque CA, Cook RJ, Browse J (1998) A role for jasmonate in pathogen defense of *Arabidopsis*. *Proc Natl Acad Sci USA* 95: 7209–7214
- Wasternack C (2014) Action of jasmonates in plant stress responses and development — Applied aspects. *Biotechnol Adv* 32: 31–39
- Würtele M, Jelich-Ottmann C, Wittinghofer A, Oecking C (2003) Structural view of a fungal toxin acting on a 14-3-3 regulatory complex. *EMBO J* 22: 987–994
- Yamaguchi Y, Huffaker A, Bryan AC, Tax FE, Ryan CA (2010) PEPR2 is a second receptor for the Pep1 and Pep2 peptides and contributes to defense responses in *Arabidopsis*. *Plant Cell* 22: 508–522
- Yang SF, Hoffman NE (1984) Ethylene biosynthesis and its regulation in higher plants. *Annu Rev Plant Physiol* 35: 155–189.
- Zarembinski TI, Theologis A (1994) Ethylene biosynthesis and action: a case of conservation. *Plant Mol Biol* 26: 1579–1597